Far-infrared studies of two-dimensional random metal-insulator composites

T. W. Noh and P. H. Song
Department of Physics, Seoul National University, Seoul, Korea

Sung-Ik Lee
Department of Physics, POSTECH, Pohang, Korea

D. C. Harris
Department of Physics, Ohio State University, Columbus, Ohio 43210

J. R. Gaines
Department of Physics and Astronomy, University of Hawaii at Manoa, Honolulu, Hawaii 96822

J. C. Garland
Department of Physics, Ohio State University, Columbus, Ohio 43210
(Received 16 March 1992)

Samples consisting of 10-μm squares of gold film (500 Å thick) are deposited as random two-dimensional (2D) arrays on sapphire substrates by using microfabrication techniques. The arrays represent a square lattice of the 2D site-percolation problem with a lattice constant of 10 μm. Far-infrared transmission and reflection spectra are measured between 8 and 92 cm^{-1}. A smooth change, rather than a sharp transition near the percolation threshold, is observed in the measured spectra. The experimental effective conductivity which is derived under the assumption that our sample looks homogeneous in the long-wavelength limit is shown to be different from the effective-medium-approximation prediction by several orders of magnitude. A scaling theory, based on the conductivity fluctuation near the percolation threshold, is found to give better description. However, there still exists a significant discrepancy between its prediction and the absorption spectra of our measurement, which we suggest is due to magnetic-dipole absorption.

I. INTRODUCTION

The optical properties of metal-insulator composites have been studied for more than a century. Most theoretical work has been based on effective-medium theories, i.e., the Maxwell-Garnett theory (MGT),[1] the effective-medium approximation (EMA),[2–5] and modifications of these two theories.[6–9] Though there has been much progress in understanding various physical properties of metal-insulator mixture near the percolation threshold,[10–14] there has been little effort[15,16] to explain their optical properties using modern percolation theories.

Recently, Yagil *et al.*[17] applied the scaling theory of percolating clusters to optical properties of semicontinuous films near the percolation threshold. In that description, the effective conductivity at finite frequencies fluctuates over the film, and the length scale of fluctuating regions is determined by the anomalous diffusion relation.[18] Instead of following the conventional approach of the effective-medium theories, i.e., using a single average effective conductivity, they used the distribution of the local conductivity to compute the optical responses of the two-dimensional (2D) films.

Scaling theory can describe the following optical properties common to the semicontinuous films near the percolation threshold:[19–21] (1) a very weak wavelength dependence in the near-ir regime, and (2) a very weak dependence of the optical responses on the volume fraction near the percolation threshold. Yagil *et al.* obtained an excellent agreement between the experimental data and numerical calculations after they included the effect of the intercluster capacitance in the simulation.[17]

In our study, we investigate the far-infrared response of a 2D random metal-insulator composite. Using modern microfabrication techniques, we make samples consisting of 10-μm squares of gold film which form 1000×1000 2D site-percolation networks. Measured transmission and reflection spectra on these artificial 2D composites between 8 and 92 cm^{-1} provide a good opportunity to compare predictions of an effective-medium theory and those of the newly developed scaling theory. Our study shows that the far-infrared responses of the 2D random composites, over a wide range of volume fractions near the percolation threshold, can be described much better by the scaling theory. This observation indicates that the far-infrared response of our 2D films near the metal-insulator transition is dominated by the conductivity fluctuation, and using a single effective conductivity in describing the far-infrared response of our composites is inadequate. Even though the scaling theory can provide a fairly good description, there still remains a significant discrepancy between its prediction and the absorption spectra of experiments. We study this

discrepancy in relation to two possible mechanisms; i.e., the capacitive coupling between the metal clusters and the magnetic dipole absorption.

The rest of this paper is organized as follows. Section II summarizes the EMA and the scaling theory. Section III describes the sample preparation techniques and the far-infrared measurements in detail. In Sec. IV, the measured far-infrared transmittance and reflectance are compared with the predictions of the EMA and those of the scaling theory. Inadequacy of the EMA in explaining the far-infrared properties of our 2D composites near the percolation threshold is demonstrated. Two possible absorption mechanisms are discussed. The summary is given in Sec. V.

II. THEORIES

A. The effective-medium approximation

Suppose that light of wavelength λ is incident on a metal-insulator composite with a typical grain size a and a conductivity which depends on position and frequency; i.e., $\sigma=\sigma(\vec{r},\omega)$. Such a local description is not very useful when the quantity of interest is the average response of the system to the incoming light. When λ is much larger than any length scale which represents inhomogeneity inside the composite, the medium looks homogeneous and its response can be described by an effective conductivity, σ_{eff}. The condition on the wavelength is usually represented by a relation, called the "long-wavelength limit,"

$$a \ll \lambda \ . \tag{1}$$

Even though this relation has been used by many workers,[4,10] it should be noted that Eq. (1) neglects other important length scales, such as cluster sizes.

The idea of the effective-medium theories is illustrated in the diagram of Fig. 1(a). Various effective-medium theories have been developed to express σ_{eff} in terms of the conductivities, volume fractions, and particle shapes of the constituents for a given composite structure. One of the most commonly used is the effective-medium approximation (EMA), which was developed by Bruggeman[2] and generalized by Stroud.[3,4] According to this theory, individual grains are considered to be surrounded by a background which represents the average response of the mixture. The self-consistent condition that there is no net extra current due to the depolarization of the grains inside the whole medium[22] gives an equation for σ_{eff}. Under the assumption that each grain is spherical in d dimensions ($d=2$ in our case) and that only the electric dipole response is important, the self-consistent equation for a two component metal-insulator composite becomes[23]

$$p\frac{\sigma_m-\sigma_{\text{eff}}}{\sigma_m+(d-1)\sigma_{\text{eff}}}+(1-p)\frac{\sigma_i-\sigma_{\text{eff}}}{\sigma_i+(d-1)\sigma_{\text{eff}}}=0 \ , \tag{2}$$

where σ_m is the conductivity of the metal, σ_i that of the insulator, and p the volume fraction of metal. The EMA predicts a metal-insulator transition, at the "percolation threshold,"[11-13] i.e., at $p=p_c=1/d=0.5$. Note that Eq. (2) does not include any variable which describes the length scale of inhomogeneity inside the composite.

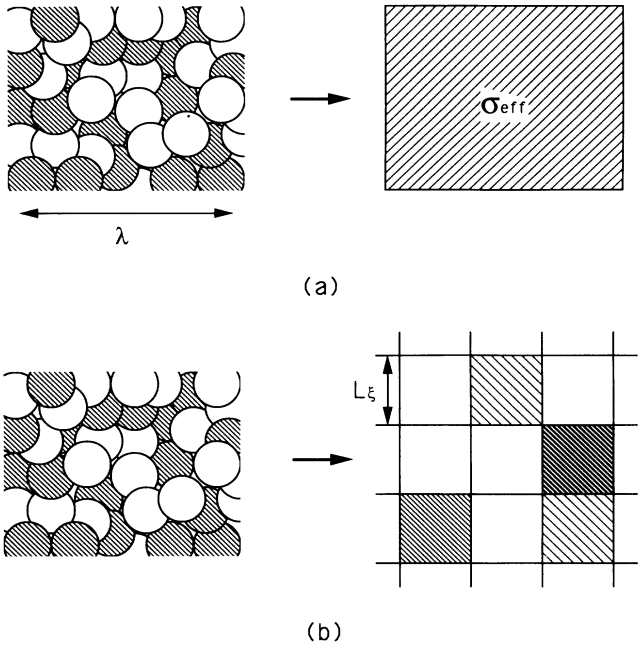

FIG. 1. (a) The approach of the effective-medium theories. When the wavelength of the incident light is much larger than any other length scales inside a composite, the response of the composite can be described by an effective conductivity σ_{eff}. (b) The approach of the scaling theory. The 2D composite is divided into the squares of linear size L_ξ. Note that there exist two kinds of squares, i.e., the squares that have metallic properties and the squares that have insulatorlike properties. The squares that have metallic properties are depicted as the hatched squares. The response of the composite is obtained by adding the local responses of the small squares.

B. Scaling theory

Near the percolation threshold, grains of the same kind form a very large cluster, so the length scale of inhomogeneity inside the composite becomes very large. In order to understand the optical properties of 2D semicontinuous metal films near p_c, Yagil *et al.*[17] have adopted a scaling theory which takes effects of the cluster formation into account.

Two different length scales, one for the inhomogeneity and a second for the measuring probe, are used in the scaling theory. The inhomogeneity length scale is represented by the coherence length ξ, which is the typical size of the finite cluster. As p approaches p_c, ξ diverges[13] with a critical exponent ν,

$$\xi=\xi_0|p-p_c|^{-\nu} \ , \tag{3}$$

where ξ_0 is of order of the lattice constant. The length of the measuring probe is represented by the anomalous diffusion length, $L(\omega)$, the distance a carrier diffuses on a cluster during the period of the electromagnetic wave

$$L(\omega)=B\xi_0(\lambda/\xi_0)^{1/(2+\theta)}\sim\omega^{-1/(2+\theta)} \ , \tag{4}$$

where B is a coefficient of order 1, and θ is the critical exponent describing the anomalous diffusion process. For the 2D percolation problem,[13,17] $\nu=\frac{4}{3}$ and $\theta=0.79$.

In the scaling theory, as shown in the diagram of Fig. 1(b), the optical response of a 2D composite is represented by the sum of the local optical responses from squares with a linear dimension of L_ξ, where L_ξ is the smaller of $L(\omega)$ and ξ. In this picture, the effective conductivity of each square is σ_j, where j is the index of the squares. Near p_c, there exists a large fluctuation in σ_j, which is described by a probability distribution function discussed later in this section.

Some squares have clusters of metal grains percolating through them so that they show a metallic behavior. The probability of finding such metallic squares is defined as f. The average value, $\sigma_{\mathrm{av}(m)}$, for the metallic squares can be expressed by a scaling function[24,25]

$$\sigma_{\mathrm{av}(m)}=\sigma_m L_\xi^{-\mu/\nu} F((\sigma_i/\sigma_m)L_\xi^{(\mu+s)/\nu}) , \quad (5)$$

where σ_m and σ_i are the conductivities of the metal and the insulator grains, respectively, and μ and s are the critical exponents describing the divergences of the dc conductivity and the dc dielectric constant, respectively.[13] All the lengths are in units of the typical grain size a, thus both $L(\omega)$ and the correlation length ξ are dimensionless. For a metal-insulator composite where $|\zeta|=|(\sigma_i/\sigma_m)L_\xi^{(\mu+s)/\nu}|\ll 1$,[26]

$$F(\zeta)=A_1+A_2\zeta . \quad (6)$$

Similarly, $(1-f)$ denotes the probability of finding insulatorlike squares, which do not have a percolating cluster of metal grains. The average value, $\sigma_{\mathrm{av}(i)}$, of such insulatorlike squares has the same functional form as Eq. (5), but

$$F(\zeta)=A_3\zeta+A_4\zeta^2 . \quad (7)$$

In Eqs. (6) and (7), the A's are constants of order 1. Note that, for dc problems, $F(\zeta)$ is equal to the constant value A_1 for metallic squares and zero for insulator like squares.

Near p_c, there exists a large fluctuation of σ_j. The details of the conductivity fluctuation are described by a probability distribution function $P(\sigma;L(\omega),\xi)$. The distribution function has been numerically studied in some detail only at $p=p_c$ (i.e., for infinite ξ), by Rammal, Lemieux, and Tremblay.[27] Their result shows that $P(\sigma;L(\omega),\xi)$ at p_c can be written as a function of a single scaling variable $z=\sigma/\sigma_{\mathrm{av}}$ and the resulting universal function can be written as $P_c(z)$. In the scaling theory, it is assumed that $P(\sigma;L(\omega),\xi)$ can be written as a scaling function, $P(\sigma;L(\omega)/\xi)$: When $L(\omega)\ll\xi$, the distribution $P(\sigma;L(\omega)/\xi)$ reduces to $P_c(z)$, but when $L(\omega)\gg\xi$, $P(\sigma;L(\omega)/\xi)$ is then a Gaussian distribution whose width scales as $[L(\omega)/\xi]^{-1}$. Note that the distribution function, in the limit of $L(\omega)\gg\xi$, is sharply peaked around σ_{av}, since $\langle(\Delta\sigma)^2\rangle/\langle\sigma\rangle^2\sim[L(\omega)/\xi]^{-2}$ approaches 0; therefore, the sample behaves as a nearly homogeneous material in this limit.

To get the average far-infrared response, such as transmittance T, of the composite medium, the response of each square must be obtained first. Then, considering the fluctuation of the transmittances, the average transmittance T can be written as

$$T=f\int T(\sigma_{\mathrm{av}(m)}(L_\xi)z)P(z;L(\omega)/\xi)dz + (1-f)\int T(\sigma_{\mathrm{av}(i)}(L_\xi)z)P(z;L(\omega)/\xi)dz , \quad (8)$$

where $T(\sigma_{\mathrm{av}(m)}(L_\xi)z)$ and $T(\sigma_{\mathrm{av}(i)}(L_\xi)z)$ are the transmittance of the metallic square and the insulatorlike square, respectively. Note that the second part of Eq. (8) is included since the complex conductivity of the insulator is not zero for the far-infrared region. An equivalent equation for the average reflectance R can be obtained by replacing the transmittance of each square with the reflectance

$$R=f\int R(\sigma_{\mathrm{av}(m)}(L_\xi)z)P(z;L(\omega)/\xi)dz + (1-f)\int R(\sigma_{\mathrm{av}(i)}(L_\xi)z)P(z;L(\omega)/\xi)dz . \quad (9)$$

Depending on the relative sizes of $L(\omega)$ and ξ, the scaling theory provides us two different optical responses. If $L(\omega)\ll\xi$, the measuring probe averages over a length scale smaller than the cluster size, so the optical response is position dependent. The optical response of the whole composite is the simple addition of local responses for areas whose typical size is about $L(\omega)$. However, if $L(\omega)\gg\xi$, the sample should look homogeneous. The distribution function of σ_j in the limit of $L(\omega)\gg\xi$ is sharply peaked around its average value, σ_{av}. Then the response of the whole medium is very close to the response of a medium which has a conductivity of σ_{av}. Therefore, the description of the scaling theory in the limit of $L(\omega)\gg\xi$ agrees with that of the effective-medium theories.

III. EXPERIMENTAL DETAILS

A. Sample preparation

Our 2D random metal-insulator composites, which represent 2D site-percolation lattices, are made using microfabrication techniques.[28] A typical sample used in our study is shown in Fig. 2(a). Our samples are 1000×1000 square lattices where, for a given value of the volume fraction, the actual sites for metal are determined by a computer generated random number sequence. The choice of unit-cell length a in our arrays is dictated by a compromise between optical parameters and an available electron-beam time. The smaller the unit size, the better our experimental condition satisfies the "long-wavelength" limit shown in Eq. (1). However, it takes a longer electron-beam time to make a sample with a smaller size of a. For these reasons, we had to choose 10 μm as the unit-cell length. In the frequency range of our experiments, i.e., from 8 to 92 cm^{-1}, the long-wavelength condition limit is satisfied.

Our masks are made using electron-beam lithographic techniques. The patterns are generated by a sequence of random numbers and transferred to the masks using a Cambridge EBMF-2-150 Electron Beam Microfabricator. During the developing and etching processes, each mask

is carefully examined under an optical microscope to screen defective masks.

To transfer the random array patterns from the masks onto the sapphire substrates, a typical photolithographic process consisting of contact printing, chlorobenzene soaking, and development[29] is used. A polycrystalline sapphire substrate $\frac{3}{4}$ in.$\times\frac{3}{4}$ in. in size (0.04 in. thick with both sides polished) is cleaned in an ultrasonic bath. The cleaned substrate is baked at 150 °C for 30 min to get better cohesion between the photoresist and the sapphire substrate. After the contact printing is done with a contact mask aligner, the photoresist is soaked with chlorobenzene for 3 min before the final developing process. This soaking process with chlorobenzene is known to provide an undercut profile of the photoresist after development.[29]

To produce 2D random gold arrays, we initially used a lift-off technique. After the random array pattern of photoresist is made on the substrates, a 500-Å-thick gold film is deposited on top of the photoresist patterns. The final 2D gold array is obtained by removing the photoresist using acetone. As can be seen from Fig. 2(b), this method gives a very clean edge to the gold square, but it suffers from a serious "corner touching" problem. The circles of Fig. 2(b) show that some of the gold lattice sites touch with their diagonally adjacent sites, but the others do not. This is very serious problem since percolation is based on connectivity. Poor control on connectivity of metal grains will give erroneous experimental results. To eliminate this "corner touching" problem, various process parameters such as exposure, developing time, and soaking time have been systematically changed. However, all these attempts were unsuccessful.

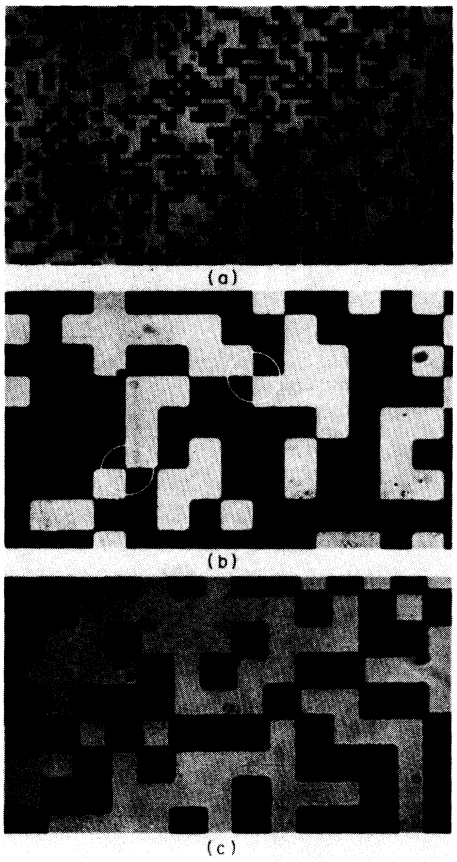

FIG. 2. (a) An optical microscope picture of a 10×10-μm^2 gold square network on sapphire. The bright squares are 500-Å-thick gold films. 1000×1000 lattice points were generated to cover the 1×1-cm^2 square. (b) An optical microscope picture of the 2D gold random array obtained by a liftoff technique. This technique produces a very clean edge to the gold film. However, as seen in the circles, the corners of the gold squares sometimes touch and sometimes do not. (c) An optical microscope picture of the 2D random array obtained after a subtractive etching. Even though the edges of the gold film are not clean, this method guarantees that the adjacent corners do not touch.

A subtractive etching technique is found to be useful to overcome the problem of "corner touching." As a first step, a gold film, 500 Å thick, is deposited on a clean sapphire substrate using thermal evaporation. Following the photolithographic techniques described earlier, a random pattern of the photoresist is produced on the gold coated substrate. Then, the random array can be obtained by chemically etching the gold film which is not covered with the photoresist. After this etching process, each sample is carefully examined under an optical microscope to check the connectivity between the adjacent squares. The chemical etching process is repeated 2–3 times until it is certain that all the metal corners are disconnected. After this process, the photoresist is removed using acetone. As we can see in Fig. 2(c), the edges of the metal squares are not as clean as those in Fig. 2(b). However, since this etching technique removes the connectivity problem, it is used in preparing our samples. The percolation threshold, p_c, is measured by the dc resistance measurement and found to be located between 0.58 and 0.60. This value is in good agreement with the well-accepted value[30] for site percolation, i.e., about 0.59. This agreement provides further evidence that the metal corners made by this technique do not touch adjacent sites. If the connectivity problem exists, the measured value of p_c should be lower than the accepted value.

B. Far-infrared measurement

The transmission and reflection spectra between 8 and 92 cm^{-1} are measured at room temperature. The reflection spectra are measured at an angle of 13°, but the transmission spectra are measured for normal incidence. The correction due to deviation from the normal incidence in the reflection spectra has been evaluated to be small, and so it is neglected in the data analysis. For both measurements, the sample is positioned in such a way that the incident beam first hits the gold film.

In the measured frequency region, the interference fringes from the sapphire substrate become very significant in both spectra. These Fabry-Perot fringes make it difficult to isolate the far-infrared properties of the film from those of the substrate. To avoid this difficulty, the spectra are measured with a very low resolution, i.e., 8 cm^{-1}.

Figure 3 shows the measured transmission and reflection spectra of our 2D metal-insulator composite

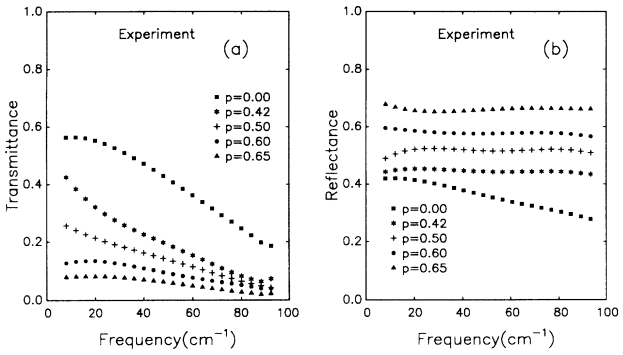

FIG. 3. (a) The measured transmission spectra of 2D random arrays with different gold volume fractions. (b) The measured reflection spectra of the same samples.

films. From Fig. 3(a), it can be seen that a metal volume fraction of $p=0.42$ is required to reduce the transmittance by a factor of 2 over that of the bare substrate around 60 cm^{-1}. Moreover, the transmittance for our 2D composite only gradually decreases as p increases. In Fig. 3(b), the reflection spectra for the composites show the opposite trend; as the volume fraction increases, the reflectance slowly increases. Note that *no drastic changes in the spectra of transmittance and reflectance are observed near the percolation threshold.*

IV. DISCUSSION

A. Intensity transfer-matrix method (ITMM)

The interference of multiply reflected beams from parallel substrate surfaces leads to Fabry-Perot fringes in the measured spectra, making the data analysis difficult. Moreover, in most real experiments, a small misalignment between the parallel surfaces causes the fringes to become smaller at high frequency, a behavior that usually cannot be explained with any reasonable model. One typical solution to this problem is to perform low resolution measurements so that the Fabry-Perot fringes cannot be seen. Then, the measured spectra should be analyzed carefully with a proper method of averaging the fringes.

One convenient technique for such data analysis is the intensity transfer-matrix method (ITMM).[31] This method neglects the phase information between the multiply reflected beams from the substrate surfaces and adds the beams incoherently, so the Fabry-Perot fringes due to the substrate do not appear. Suppose that light enters a thin film from the left side, as shown in Fig. 4(a). The thickness of the substrate is t. In the ITMM, six different optical responses, shown in Fig. 4(b), are used. If the substrate were of infinite thickness, the transmittance and the reflectance of the film for the light entering from the left side would be T_a and R_a, respectively. For the light entering from the opposite direction, the corresponding terms are denoted by T_a' and R_a'. The other two optical responses are T_b and R_b, the transmittance and the reflectance of the interface between the air and the substrate for the light entering from the substrate side. These six optical responses are obtained by solving the Maxwell's equation exactly,[32] i.e., the multiply reflected beams in the thin film are added coherently.

The reflectance of the film is obtained by summing the intensity of light traveling along the various paths; in other words,

$$R=R_a+T_aT_a'R_be^{-2\alpha t}+T_aT_a'R_a'R_b^2e^{-4\alpha t}+\cdots$$
$$=R_a+\frac{T_aT_a'R_b\exp(-2\alpha t)}{1-R_a'R_b\exp(-2\alpha t)}\ , \tag{10}$$

where α is the absorption coefficient of the substrate. After a similar calculation for the transmittance, we get

$$T=\frac{T_aT_b\exp(-\alpha t)}{1-R_a'R_b\exp(-2\alpha t)}\ . \tag{11}$$

Note that the phase information between the multiply reflected beams in the substrate is neglected in Eqs. (10) and (11).

To check the validity of the ITMM, a numerical simulation was used. For arbitrary values of conductivities and thicknesses of the film and the substrate, the transmission and the reflection spectra were evaluated exactly.[32] To eliminate the Fabry-Perot fringes, the calculated spectra for a given frequency were averaged with a proper weighted function, for example, a triangular win-

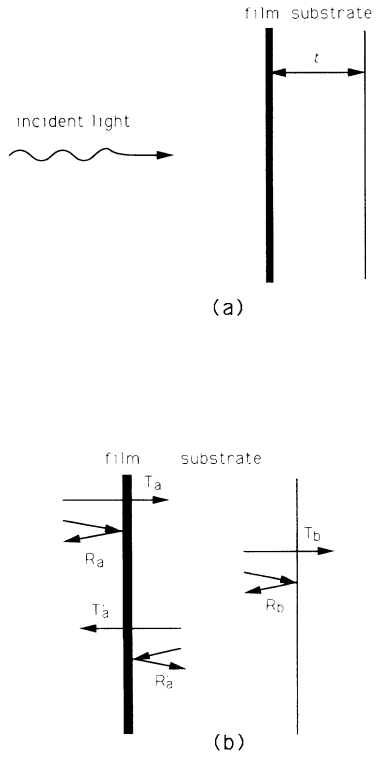

FIG. 4. Schematic diagrams for the intensity-transfer matrix method (ITMM). (a) Light is incident normally on a thin film which is on top of a thick substrate. The thickness of the substrate is t. (b) Six optical responses required in the ITMM are indicated. The arrows designate the direction of light.

dow. The width of the weighted function was chosen to give the resolution of 8 cm^{-1}. (This process is similar to measuring spectra with a low resolution.) These averaged spectra agreed with the prediction of ITMM.

B. FIR optical constants of fused sapphire

From Fig. 3, it is apparent that the bare sapphire substrate absorbs far-infrared (FIR) radiation rather strongly at room temperature, especially in the high-frequency region near 90 cm^{-1}. This absorption is too strong to be neglected in our data analysis.

The complex index of refraction, $\tilde{n}_s$ ($=n_s+ik_s=\sqrt{\epsilon_s}$), for polycrystalline sapphire is calculated from the experimental transmission and reflection spectra for the bare substrate. The ITMM, combined with a proper numerical technique, is used to find $\tilde{n}_s$. In this case, since there is no gold film on the substrate, the six optical responses in Eqs. (10) and (11) should be modified appropriately. Generally speaking, the transmittance when light is incident on an absorbing medium from air is different from that when light is incident on air from the absorbing medium. However, when the real part of the index of refraction for the absorbing medium is much larger than its imaginary part, $T_a \cong T_a' = T_b$ and $R_a = R_a' = R_b$. The real and imaginary parts of $\tilde{n}_s$ are plotted in Fig. 5. The open circles in Fig. 5 indicate the measured n_s, which is nearly constant up to 90 cm^{-1}. The reported values for a single crystalline sapphire[33] are also plotted. The dashed line is n_s for the ordinary ray, and the dotted line is that for the extraordinary ray. Our measured values for polycrystalline sapphire are located between these two lines. The open triangles in Fig. 5. show that the experimental value of k_s increases with frequency. The magnitude of k_s is large enough to affect the spectra of our 2D films significantly.

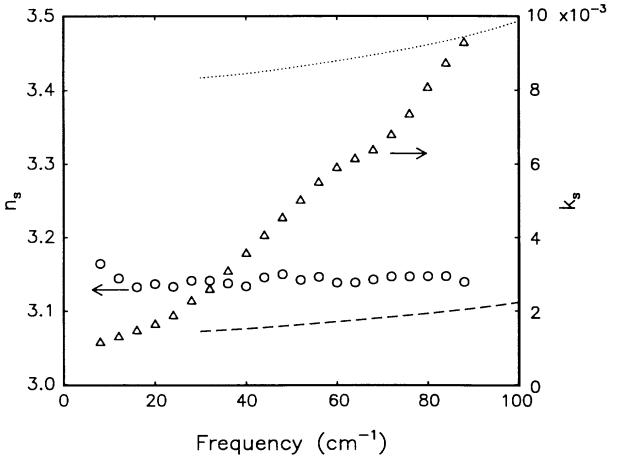

FIG. 5. The index of refraction for polycrystalline sapphire. The open circles represent the real part of the index of refraction, n_s. (The scale of these points is indicated on the left y axis.) For comparison, the values for crystalline sapphire are plotted as a dashed line (for the ordinary ray) and a dotted line (for the extraordinary ray). The open triangles represent the imaginary part of the index of refraction, k_s. (The scale of k_s is shown on the right y axis.)

C. Comparison with the EMA predictions

In the EMA calculation, the conductivity of gold is represented by the simple Drude model

$$\sigma(\omega)=\frac{\sigma_{dc}}{1-i\omega\tau}\ , \tag{12}$$

where the dc conductivity σ_{dc} is taken to 3.5×10^{17} sec^{-1}, and the relaxation time τ is 2×10^{-15} sec[34]. Since there is no material between the metal clusters, $\epsilon_i=(4\pi i/\omega)\sigma_i$, the dielectric constant of the insulator, is taken to be 1. The effective conductivities for our 2D films are calculated from Eq. (2).

With the measured optical constants for fused sapphire and σ_{eff} obtained from Eq. (2), the theoretical transmittance and reflectance are obtained using Eqs. (10) and (11). The EMA results, shown in Fig 6, predict very abrupt changes near p_c. For a sample with $\Delta p=p-p_c=0.01$, the transmittance becomes very small and the reflectance approaches one. This predicted behavior is not observed in our experimental data, i.e., Fig. 3.

This large discrepancy between the experimental results and the EMA predictions is due to the fact that the EMA treats the composite as a homogeneous material with a single effective conductivity. The EMA predictions on the real part of the effective conductivity are plotted in Fig. 7(a). For samples with $\Delta p=-0.01$ and $\Delta p=0.01$, the EMA predicts changes in the effective conductivity by more than eight orders of magnitude.

To see how far these EMA predictions are from the experimental observations, we numerically calculate the effective conductivities of our samples under the assumption that the optical response of our film for a given volume fraction can be represented by a single value of σ_{eff}. The σ_{eff} of the film was obtained from the ITMM. This hypothetical quantity, plotted in Fig. 7(b), changes by less than one order of magnitude over most of the experimental frequency range even though Δp varies from -0.20 to 0.06. The large differences between curves in Figs. 7(a) and 7(b) show that the EMA cannot properly describe the far-infrared response of our films.

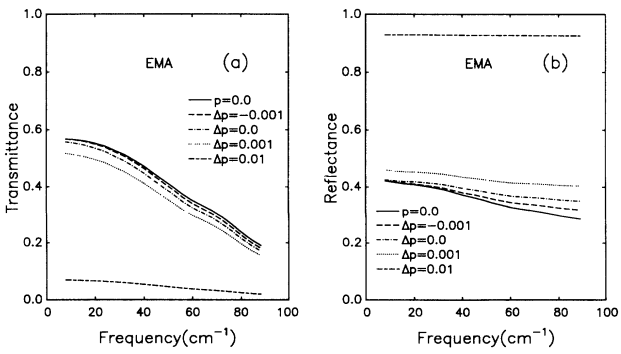

FIG. 6. (a) The transmission spectra predicted by the EMA. (b) The reflection spectra predicted by the EMA.

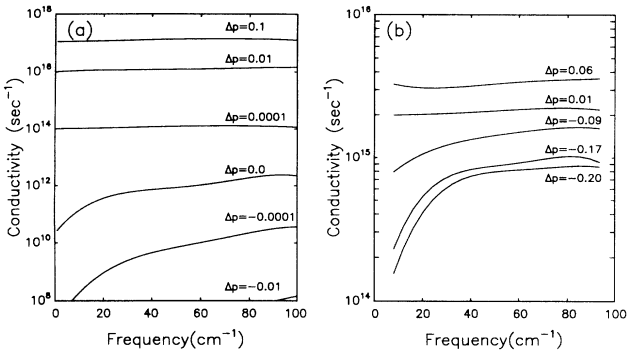

FIG. 7. The real part of the effective far-infrared conductivity of our 2D random arrays with different volume fractions of gold: (a) the EMA predictions and (b) our measurement. The experimental values are obtained under the assumption that the samples appear homogeneous. Note the large differences between the EMA predictions and the experimental values.

The above-mentioned failure of the EMA comes from the fact that the effective medium theory treats our samples as a homogeneous medium. Even though the long-wavelength limit as defined by Eq. (1) is satisfied in our experiments, the approach of the EMA clearly fails. Near the percolation threshold, the coherence length becomes very large, so the length scale of the measuring probe becomes comparable to or shorter than the length scale of sample inhomogeneity, so that the local far-infrared response strongly depends on the position of the incident light. This is accounted for by the scaling theory, as explained in Sec. II B.

D. Comparison with the scaling theory predictions

It is necessary to know the probability of finding metallic squares in the scaling theory. Yagil *et al.*[17] estimated the probability from another scaling equation such as

$$f-f_c=u_{\pm}[L_{\xi}/\xi_0^{(\pm)}]^{1/\nu}(p-p_c)\ , \tag{13}$$

where $\xi_0^{(+)}$ and $\xi_0^{(-)}$ are the amplitudes of the coherence length above and below p_c, respectively, and u_+ and u_- are the corresponding coefficients, respectively. When dual symmetry for $p>p_c$ and $p<p_c$ exists (for example, the 2D bond-percolation problem), $\xi_0^{(+)}=\xi_0^{(-)}$ and $u_+=u_-$. When dual symmetry does not exist, $\xi_0^{(+)}$ and $\xi_0^{(-)}$ can be obtained by numerical simulation, and the other parameters can be obtained from the following equations:

$$f_c=\frac{(\xi^{(-)})^{1/\nu}}{(\xi^{(+)})^{1/\nu}+(\xi^{(-)})^{1/\nu}}\ ,$$
$$u_-=f_c\ , \tag{14}$$

and

$$u_+=1-f_c\ .$$

We could find no values for $\xi_0^{(+)}$ and $\xi_0^{(-)}$ for 2D site percolation in the literature, so we set $\xi_0^{(+)}=1$, $\xi_0^{(-)}=1$, and $p_c=0.59$ in our calculation. However, we found that changing the values of $\xi_0^{(+)}$ and $\xi_0^{(-)}$ by a factor 2 does not affect our numerical results significantly.

We estimated $\sigma_{\mathrm{av}(m)}(L_{\xi})$ and $\sigma_{\mathrm{av}(i)}(L_{\xi})$ from Eqs. (5), (6), and (7). In these evaluations, the geometry-dependent coefficients, such as A_1, A_2, A_3, and A_4 are also set equal to 1. Changes in these parameters do not significantly influence our theoretical curves either.

The transmittance and reflectance for a given square can be calculated using the ITMM, i.e., Eqs. (10) and (11). The distribution function $P(\sigma;L(\omega)/\xi)$ in the region of $L(\omega)<\xi$ is estimated by fitting the numerical results by Rammal, Lemieux, and Tremblay[27] with a double-log-normal distribution. To provide a smooth change in the far-infrared response from the region of $L(\omega)<\xi$ to that of $L(\omega)>\xi$, the same functional form for $P(\sigma;L(\omega)/\xi)$ is used in the region of $L(\omega)>\xi$, but with a much sharper distribution width of $\langle(\Delta\sigma)^2\rangle/\langle\sigma\rangle^2\sim[L(\omega)/\xi]^{-2}$. Even though this distribution is not a Gaussian, the scaling theory predictions remain unchanged.

The results of scaling theory are shown in Fig. 8. Comparison of these results with Figs. 3 and 6 shows that scaling theory is much better than the EMA in describing the far-infrared responses of our 2D random composites. The abrupt changes near p_c predicted by the EMA appear neither in this calculation nor in the experimental data.

E. A remaining puzzle in the absorption spectra

Even though the scaling theory can provide a much better description of our experimental data than the EMA, there still remains an important discrepancy between the experimental data and the scaling theory predictions. A careful look on Figs. 3 and 8 reveals that both transmittance and reflectance, as predicted by the scaling theory, are larger than experimental values. In particular, the theoretical transmittances are two to three times larger than the experimental values.

The discrepancy can be seen most clearly in the absorption spectra. Figure 9 shows the experimental and theoretical absorption spectra. The measured absorption spectra, shown in Fig. 9(a), are larger than the prediction of scaling theory, shown in Fig. 9(b), for all the samples

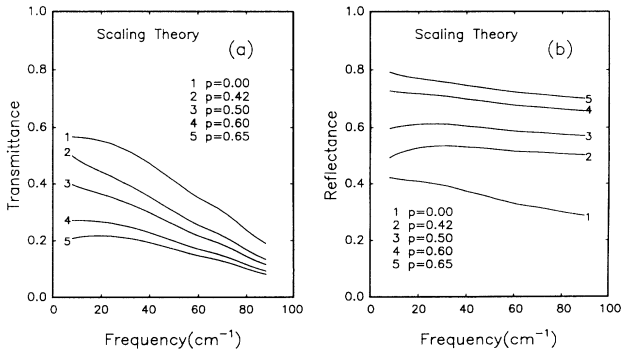

FIG. 8. (a) The transmission spectra calculated by the scaling theory. (b) The reflection spectra calculated by the scaling theory.

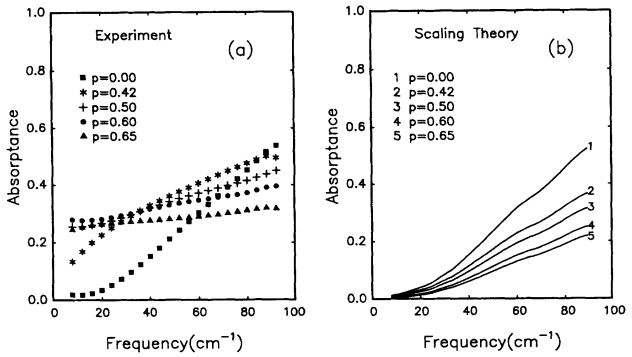

FIG. 9. (a) The measured absorption spectra. (b) The absorption spectra calculated by the scaling theory.

with $p \geq 0.42$. In the high-frequency region, the experimental absorptance decreases as the volume fraction increases, in qualitative agreement with scaling theory. However, in the low-frequency region, the measured absorptance shows an enhancement as p increases, which is opposite to the theoretical prediction.

For more insight into these absorption spectra, we calculate theoretical transmission and reflection spectra for a hypothetical 2D random composite with no substrate, and obtain the absorptance, i.e., $(1-T-R)$. The results are shown in Fig. 10. The scaling theory shows that the absorption loss in the free-standing sample is less than 1% of that for the sample, with any volume fraction. This fact clearly shows that the calculated absorption loss in Fig. 9(b) is due to the substrate. The monotonic decrease of the absorptance shown in Fig. 9(b) is due to the fact that for a sample with a higher volume fraction there is a smaller probability that the light meets the bare substrate without experiencing reflection. The similar behavior of the measured absorptance in the high-frequency region can be explained by the same argument.

However, the behavior of the measured absorptance in the low-frequency region indicates that some other far-infrared absorption mechanism exists. We consider two different mechanisms which could account for the far-infrared absorption losses; absorption due to capacitive coupling between metal clusters, and magnetic-dipole absorption.

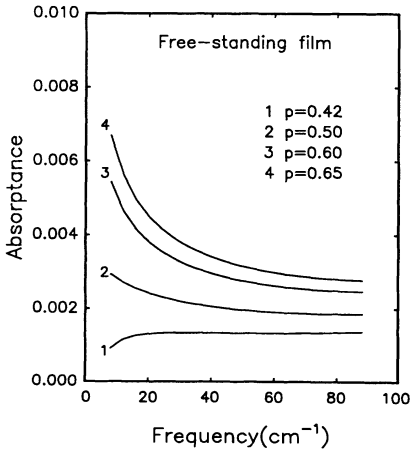

FIG. 10. Absorption spectra for hypothetical samples which have exactly the same geometry as our 2D random composites but without the sapphire substrate. Note that the maximum of the y axis is 0.01 instead of 1.0.

1. *Capacitive coupling between metal clusters*

Metal clusters located very close to each other can have significant capacitive coupling. Yagil *et al.*[17] included such capacitive coupling to explain their large experimental absorption of the semicontinuous gold films near p_c. However, the coupling in our 2D samples is not as large as that of the semicontinuous films. The lattice constant of our sample is 10 μm, much larger than the typical dimension ($\sim$300 Å) of gold grains in the semicontinuous film. Therefore, the coupling between the metal clusters in our sample should be much smaller than that for the semicontinuous film.

To understand the effects of capacitive coupling more quantitatively, they are introduced in the scaling theory. The coupling is incorporated using the conductivity of the insulator, such as

$$\sigma_i = i\omega C_0 \ , \tag{15}$$

where C_0 is of the order of the capacitance per unit thickness between two adjacent metal grains. For simplicity, C_0 is assumed to be frequency independent. A relatively good fit for the transmission spectrum of the sample with $p=0.65$ is obtained for the choice $C_0=10$. This value is about ten times larger than the value used by Yagil *et al.*, which is contradictory to our earlier argument.

The scaling theory predictions with $C_0=10$ are plotted in Fig. 11. Comparison between Figs. 8(a) and 11(a) shows that the transmittance is suppressed by capacitive coupling. On the other hand, comparison between Figs. 8(b) and 11(b) shows that the reflectance is enhanced by the coupling. Changes due to the capacitive coupling become larger at the higher frequency regions, as expected by Eq. (15). The absorption spectra calculated by $(1-T-R)$ shows that capacitive coupling makes the ab-

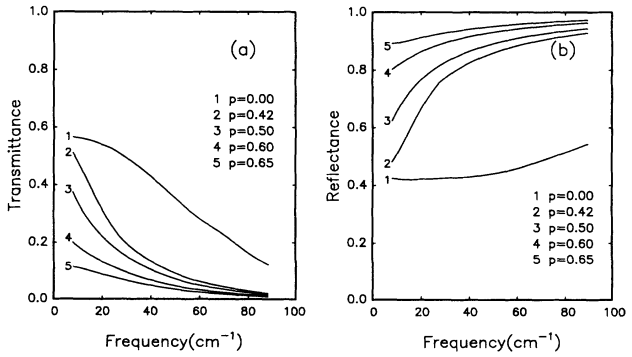

FIG. 11. The calculated spectra using the scaling theory when capacitive coupling is included. (a) Transmission spectra. (b) Reflection spectra.

sorptance even smaller than the value calculated without the coupling. This result shows that the capacitive coupling between the metal clusters cannot explain the anomalous large far-infrared absorption observed in our experiment.

2. *Magnetic dipole absorption*

In both the EMA and the scaling theory, only the absorption due to the electric dipole is included. The electric dipole absorption *is* the most important absorption mechanism in most cases. However, for some cases, the magnetic dipole absorption due to eddy currents,[35,36] which causes the medium to have a nonzero magnetization even though the constituents are nonmagnetic, has been shown to play an important role.[37–40] For examples, in the far-infrared region, the magnetic dipole absorption becomes several order of magnitude larger than the electric dipole absorption for metal particles of size 1000 Å.[41] The magnetic dipole absorption can be described by a competition between the absorbing power (i.e., a term related to the conductivity) and the absorbing volume (i.e., a term related to the skin depth), so it depends strongly on the size of the particles and the frequency of measurement. Therefore, clustering of small particles has been shown to be important in some far-infrared absorption experiments.[38,40] Considering that the skin depth of gold is comparable to our film thickness, the magnetic dipole absorption could be very significant in our experiment. The eddy current effects are very difficult to handle since the governing equation is no longer the Laplace equation, but the Helmholtz equation. There are a few theoretical results on the magnetic-dipole absorption that include the effect of cluster formation, but their results are not consistent. Both numerical models[42,43] and a scaling theory[44] predict a divergent response at p_c. However, a recent treatment that takes mutual inductance into account does not show divergent behavior.[45]

We suggest that the discrepancy between the experimental absorption spectra, shown in Fig. 9(a), and that of the scaling theory, shown in Fig. 9(b), is due to magnetic-dipole absorption. Since our experiments represent far-infrared measurements on lattices of the 2D site-percolation problem, our experimental results can be compared with computer simulations without any free parameters. Further investigation of the observed discrepancy in the absorption spectra may provide an opportunity for us to understand the effects of cluster formation on the magnetic dipole absorption near the percolation threshold.

V. SUMMARY

The far-infrared transmittance and reflection spectra have been recorded for samples which represent a 1000×1000 2D site-percolation problem. The EMA cannot explain our experimental observations, but an approach based on a scaling theory gives a more reasonable description of our experimental results. This improved agreement demonstrates that the fluctuation of local conductivities near the percolation threshold influences the far-infrared response of our 2D films. However, there remains an important difference between the absorption spectra of our experiment and those predicted by scaling theory. We suggest that the origin of this discrepancy is neglect of the magnetic dipole absorption in the calculation.

ACKNOWLEDGMENTS

We would like to thank our colleague David Stroud for his many useful discussions. This research was supported by the National Science Foundation through Grant Nos. DMR 87-16520 and DMR 88-21167, as well as through support provided the National Research and Resource Facility for Submicron Structures. The work at SNU was supported by the Korea Science and Engineering Foundation (KOSEF) through the Science Research Center (SRC) of Excellence Program and by the Ministry of Education through the Basic Science Research Institute program.

[1] J. C. Maxwell Garnett, Philos. Trans. R. Soc. London **203**, 385 (1904).
[2] D. A. G. Bruggeman, Ann. Phys. (Leipzig) **24**, 636 (1935).
[3] D. Stroud, Phys. Rev. B **12**, 3368 (1975).
[4] D. Stroud and F. P. Pan, Phys. Rev. B **17**, 1602 (1978).
[5] D. Stroud, Phys. Rev. B **19**, 1783 (1979).
[6] P. Sheng, Phys. Rev. Lett. **45**, 60 (1980).
[7] U. J. Gibson, H. G. Craighead, and R. A. Buhrman, Phys. Rev. B **25**, 1449 (1982).
[8] J. V. Mantese, W. A. Curtin, and W. W. Webb, Phys. Rev. B **33**, 9897 (1986).
[9] M. F. MacMillan, R. P. Devaty, and J. V. Mantese, Phys. Rev. B **43**, 13 838 (1991).
[10] *Proceedings of the First Conference on the Electrical Transport and Optical Properties of Inhomogeneous Media, Ohio State University, 1977,* edited by J. C. Garland and D. B. Tanner (AIP, New York, 1978).
[11] D. Stauffer, Phys. Rep. **54**, 1 (1979).
[12] *Percolation Structures and Processes,* edited by G. Deutscher, R. Zallen, and J. Adler (Hilger, Bristol, 1983).
[13] D. Stauffer, *Introduction to Percolation Theory* (Taylor & Francis, London, 1985).
[14] T. W. Noh, Y. Song, S.-I. Lee, J. R. Gaines, H. D. Park, and E. R. Kreidler, Phys. Rev. B **33**, 3793 (1986).
[15] G. A. Niklasson and C. G. Granqvist, Phys. Rev. Lett. **56**, 256 (1986).
[16] R. P. Devaty, Phys. Rev. B **44**, 593 (1991).
[17] Y. Yagil, M. Yosefin, D. J. Bergman, and G. Deutscher, Phys. Rev. B **43**, 11 342 (1991).
[18] Y. Gefen, A. Aharony, and S. Alexander, Phys. Rev. Lett. **50**, 77 (1983).
[19] Y. Yagil and G. Deutscher, Appl. Phys. Lett. **52**, 373 (1988).
[20] P. Gadenne, Y. Yagil, and G. Deutscher, Physica A **157**, 279 (1989).
[21] T. Robin and B. Souillard, Physica A **157**, 285 (1989).
[22] T. W. Noh, P. H. Song, and A. J. Sievers, Phys. Rev. B **44**,

5459 (1991).
[23]R. Landauer, in *Proceedings of the First Conference on the Electrical Transport and Optical Properties of Inhomogeneous Media, Ohio State University, 1977* (Ref. 10), p. 17.
[24]J. P. Straley, J. Phys. C **9**, 783 (1976); **13**, 819 (1980).
[25]H. E. Stanley, P. J. Reynolds, S. Redner, and F. Family, in *Real Space Renormalization,* edited by T. W. Burkhardt and J. M. J. Van Leeuwen (Springer, Berlin, 1982).
[26]D. Stroud and D. J. Bergman, Phys Rev. B **25**, 2061 (1982).
[27]R. Rammal, M. A. Lemieux, and A. M. S. Tremblay, Phys. Rev. Lett. **54**, 1087 (1985).
[28]D. E. Prober, in *Percolation, Localization and Superconductivity,* edited by A. M. Goldman and S. A. Wolf (Plenum, New York, 1983), p. 231.
[29]G. G. Collins and C. W. Halsted, IBM J. Res. Dev. **26**, 596 (1982).
[30]S. Kirkpatrick, in *Proceedings of the First Conference on the Electrical Transport and Optical Properties of Inhomogeneous Media, Ohio State University, 1977* (Ref. 10), p. 99.
[31]C. J. Gabriel and A. Nedoluha, Opt. Acta **18**, 415 (1971).
[32]M. Born and E. Wolf, in *Principles of Optics,* 6th ed. (Pergamon, Oxford, 1980), p. 628.
[33]E. V. Lowenstein, D. R. Smith, and R. L. Morgan, Appl. Opt. **12**, 398 (1973).
[34]M. L. Theye, Phys. Rev. B **2**, 3060 (1970).
[35]L. D. Landau and E. M. Lifshitz, in *Electrodynamics of Continuous Media* (Pergamon, New York, 1960), Secs. 72 and 73.
[36]W. R. Smythe, *Static and Dynamic Electricity,* 2nd ed. (McGraw-Hill, New York, 1950), Chap. 11.
[37]P. N. Sen and D. B. Tanner, Phys. Rev. B **26**, 3582 (1982).
[38]W. A. Curtin, R. C. Spitzer, N. W. Ashcroft, and A. J. Sievers, Phys. Rev. Lett. **54**, 1071 (1985).
[39]W. A. Curtin and N. W. Ashcroft, Phys. Rev. B **32**, 3287 (1985).
[40]T. W. Noh, S.-I. Lee, and J. R. Gaines, Phys. Rev. B **33**, 1401 (1986).
[41]N. E. Russell, J. C. Garland, and D. B. Tanner, Phys. Rev. B **23**, 632 (1981).
[42]R. Rammal and J. C. Angles d'Auriac, J. Phys. C **16**, 3933 (1983).
[43]D. R. Bowman and D. Stroud, Phys. Rev. Lett. **52**, 299 (1984).
[44]R. Rammal, T. C. Lubensky, and G. Toulouse, J. Phys. (Paris) Lett. **44**, L65 (1983).
[45]A. N. Lagar'kov, L. V. Panina, and A. K. Sarychev, Zh. Eksp. Teor. Fiz. **93**, 215 (1987) [Sov. Phys. JETP **66**, 123 (1987)].

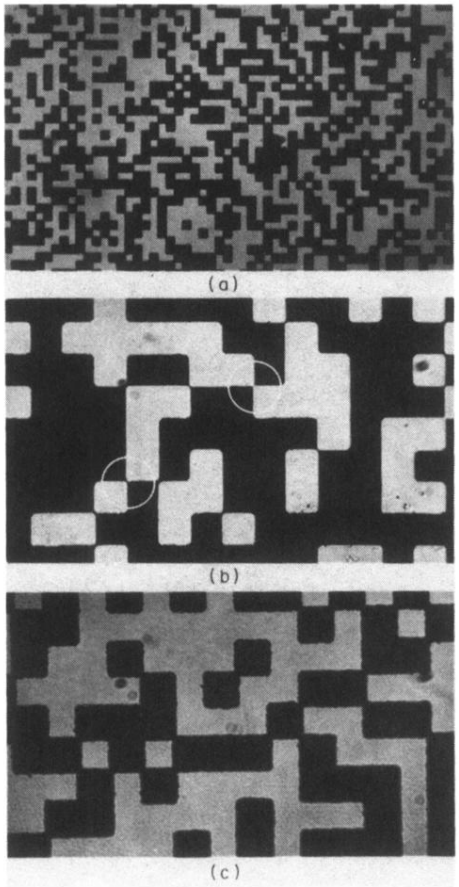

FIG. 2. (a) An optical microscope picture of a 10×10-μm^2 gold square network on sapphire. The bright squares are 500-Å-thick gold films. 1000×1000 lattice points were generated to cover the 1×1-cm^2 square. (b) An optical microscope picture of the 2D gold random array obtained by a liftoff technique. This technique produces a very clean edge to the gold film. However, as seen in the circles, the corners of the gold squares sometimes touch and sometimes do not. (c) An optical microscope picture of the 2D random array obtained after a subtractive etching. Even though the edges of the gold film are not clean, this method guarantees that the adjacent corners do not touch.